Perspective

Sustainability Strategy for the Cool Copper Collider

Martin Breidenbach,[1,2] Brendon Bullard,[1] Emilio Alessandro Nanni,[1,2] Dimitrios Ntounis,[1,2] and Caterina Vernieri[1,2,*]

[1] *SLAC National Accelerator Laboratory, 2575 Sand Hill Road, Menlo Park, California 94025, USA*
[2] *Stanford University, 450 Jane Stanford Way, Stanford, California 94305, USA*

(Received 17 July 2023; published 26 October 2023)

The particle physics community has agreed that an electron-positron collider is the next step for continued progress in this field, giving a unique opportunity for a detailed study of the Higgs boson. Several proposals are currently under evaluation by the international community. Any large particle accelerator will be an energy consumer and so, today, we must be concerned about its impact on the environment. This paper evaluates the carbon impact of the construction and operation of one of these Higgs factory proposals, the Cool Copper Collider. It introduces several strategies to lower the carbon impact of the accelerator. It proposes a metric to compare the carbon costs of Higgs factories, balancing physics reach, energy needs, and carbon footprint for both construction and operation, and compares the various Higgs factory proposals within this framework. For the Cool Copper Collider, the compact 8 km footprint and the possibility for cut-and-cover construction greatly reduce the dominant contribution from embodied carbon.

DOI: 10.1103/PRXEnergy.2.047001

I. INTRODUCTION

An electron-positron collider gives a unique opportunity to study the Higgs boson's properties with unprecedented precision and also provides an exceptionally clean environment to search for subtle new physics effects [1]. A number of different "Higgs factory" (HF) proposals, based on linear and circular colliders, are now under consideration. All of these provide e^+e^- collisions at center-of-mass energies $(\sqrt{s})$ in the range of 240–370 GeV, and some are also capable of reaching higher energies.

A high-energy particle collider is a large energy-consuming research facility. Therefore, it is important to balance its scientific importance against its environmental cost. The environmental impact of large accelerators has been analyzed in the recent Snowmass 2021 study [2] of the future of particle physics in the USA [3–5]. References [4,6–8] have examined the environmental cost of particular Higgs factory proposals, although often concentrating on particular elements of the total cost.

In this paper, we attempt a comprehensive evaluation of the carbon cost of the Cool Copper Collider (C^3) Higgs factory proposal [9,10] over its full lifetime, including costs from construction and from operation over the proposed timeline. This paper is structured as follows: In Sec. II, we briefly review the design of C^3. In Sec. III, we review the physics reach for C^3 and other Higgs factory proposals and introduce a metric for balancing carbon impact against the physics impact of each proposal. In Sec. IV, we analyze the power costs of operation of C^3 and describe methods for modifying the power design of the accelerator that would lead to substantial savings with little impact on the physics performance. In Sec. V, we analyze the carbon impact of the construction of C^3 and emphasize that cut-and-cover construction, as opposed to construction in a deep tunnel, has significant advantages. In Sec. VI, we discuss options for the source of electrical power for the C^3 laboratory. In Sec. VII, we bring these analyses together to estimate the total carbon footprint of C^3. Using information from available studies and design reports, we estimate the carbon impact of other Higgs factory proposals and compare these with C^3 in the framework described in Sec. III.

II. REVIEW OF THE C^3 ACCELERATOR DESIGN

C^3, which was proposed recently [9,10], is a linear facility that will first operate at 250 GeV center-of-mass collisions. Immediately afterward, without further extension of the linac, it will run at 550 GeV with an rf power upgrade.

*caterina@slac.stanford.edu

TABLE I. Target beam parameters for C^3.

Parameter	Value	
$\sqrt{s}$ (GeV)	250	550
Luminosity (cm^{-2} sec^{-1})	1.3×10^{34}	2.4×10^{34}
Number of bunches per train	133–200	75
Train repetition rate (Hz)	120	120
Bunch spacing (ns)	5.3–3.5[a]	3.5
Site power (MW)	150	175
Beam power (MW)	2.1	2.45
Gradient (MeV/m)	70	120
Geometric gradient (MeV/m)	63	108
rf pulse length (ns)	700	250
Shunt impedance (MΩ/m)	300	300
Length (km)	8	8

[a]Beam dynamics and structure optimization studies are ongoing: the injected charge range is between 0.7 and 1 nC with a bunch spacing ranging between 3.5 and 5.3 ns and final horizontal beam size ranging between 156.7 and 182 nm, without changes to the instantaneous luminosity. Accelerating structure optimization studies include varying a/λ from 0.05 to 0.07 with π-$2\pi/3$ phase advance [13] to reduce the longitudinal wakefield and preserve the shunt impedance.

High-energy operation will enable the exploration of the Higgs boson–top quark coupling, and will provide direct access to the Higgs boson self-coupling with double Higgs boson production [10,11]. Furthermore, the beam polarization, which exploits the strong dependence of electroweak processes on the chirality of the initial-state particles, will offer unique insights into the underlying physics, acting as a new tool for discovery [12]. This offers C^3 strong complementarity with proton and circular e^+e^- colliders, where beam polarization is not possible.

For C^3, an approach radically different from the one adopted for linacs is used to build a collider with high gradient and high rf efficiency and thus lower capital and operating costs [13]. C^3 is based on a distributed coupling accelerator concept, running under liquid nitrogen [14], that has led to an optimized accelerating gradient and minimized breakdown problems with respect to earlier designs based on normal conducting technologies. This has yielded an overall optimization of the gradient at 70 and 120 MeV/m for the 250 and 550 GeV operating points, respectively [15]. Much higher energies are possible if length is not the major consideration. The fundamental C^3 parameters, assumed for the analysis in this paper, are shown in Table I.

By far the major development to date is the actual distributed coupling accelerator structure. C^3 will use C-band (5.712 GHz) standing wave rf accelerating structures that are 1 m long. Each has an rf waveguide to bring power in, and in the more probable operating modes, each splits rf power evenly between the beam and dissipation in the structure with 43% beam loading. Operation at 80 K brings the shunt impedance up to 300 MΩ/m, allowing efficient operation at 120 MeV/m. These gradients have been demonstrated at C-band [16] and with an electron beam in an X-band (11.424 GHz) structure on the SLAC XTA beamline [14]. The C-band structure has been tested at low power at SLAC and at high power without a beam at Radiabeam [17]. The C^3 gradient results in a collider with a 550 GeV center-of-mass energy capability on an 8 km footprint.

A preconceptual design for the overall linac cryogenic system has been developed that includes the design for the cryomodules. For the C^3 250 and 550 GeV design, each linac will have three reliquification cryoplants. Liquid nitrogen will flow out along the linac in both directions, so there are six flow runs. The liquid nitrogen will be above the raft structures, with an initial velocity of approximately 0.03 m/s. The liquid nitrogen will cool the accelerator structures by nucleate boiling with a power density of 0.4 W/cm^2, producing saturated vapor that counterflows back to the cryoplant. Each cryorun is about 450 m long. The vapor velocity near the cryoplant is approximately 3 m/s.

III. COMPARISON OF HIGGS FACTORY PHYSICS REACH

Among the e^+e^- colliders being evaluated by the community, the International Linear Collider (ILC) [12,18], based on superconducting rf technology, has the most advanced design [19], and it is currently under consideration for construction in Japan. CERN is pursuing as its main strategy a large circular collider, the Future Circular Collider (FCC) [20], and China is planning a similar circular collider, the Circular Electron-Positron Collider (CEPC) [21]. Each of these circular colliders would require a tunnel with circumference on the order of 100 km to limit synchrotron radiation. However, the expected instantaneous luminosity drops off significantly above center-of-mass energies of 350–400 GeV. An alternative strategy is to construct a compact linear e^+e^- collider based on high-gradient acceleration. CERN is also pursuing such a proposal, the Compact Linear Collider (CLIC) [22], that would operate at a collision energy of 380 GeV.

The carbon footprint of the proposed future Higgs factories should be assessed relative to the expected physics reach, which has been reviewed most recently in the context of the Snowmass Process [1,23]. The primary physics goal of a future Higgs factory is the determination of the total Higgs width and Higgs couplings with percent or subpercent precision. A reasonable figure of merit to gauge the physics reach of each machine is the expected level of precision for each of these measurements. We note that evaluating the projected measurement precision accounts

for the fact that different beam configurations (center-of-mass energy and beam polarization) have a strong impact on the physics reach of each of those machines. These differences in precision are not accounted for when one is comparing the total number of Higgs bosons produced alone [1,12].

The physics reach at e^+e^- colliders increases with the center-of-mass energy, since different Higgs boson production mechanisms become accessible. At 250 GeV center-of-mass energy operation, the main Higgs boson production mechanism is associated production with a Z boson ($e^+e^- \to ZH$), enabling a model-independent determination of the Higgs boson total width. Higgs boson production via the W-boson fusion reaction $e^+e^- \to \nu\bar{\nu}H$ is accessible at $\sqrt{s} \sim 500$ GeV, where the only visible signals in the final state come from Higgs boson decays. This allows Higgs boson measurements governed by different systematic effects, complementary to the 250 GeV data, as well as opportunities to study effects such as separation of $H \to gg/b\bar{b}/c\bar{c}$ decays and CP violation in $H \to \tau^+\tau^-$ [12]. Importantly, at high center-of-mass energies, double Higgs boson production in the ZHH channel opens up, providing direct access to the Higgs boson self-coupling λ_3. Direct constraints on the top quark Yukawa coupling y_t also become accessible via $e^+e^- \to t\bar{t}H$ production at $\sqrt{s}$ above approximately 500 GeV. At circular machines, given the energy limitations, double Higgs boson and associated top quark production mechanisms are not accessible, thus allowing only indirect and model-dependent measurements of λ_3 and y_t, both through loop effects in single Higgs boson production.

The use of longitudinal beam polarization offers unique advantages for effective precision measurements at a linear e^+e^- collider, since the interaction cross sections at an e^+e^- collider have strong dependencies on beam polarization. It has been demonstrated that at 250 GeV center-of-mass energy, the ultimate precision reach in the determination of Higgs couplings, through a Standard Model effective field theory (SMEFT) analysis, for an integrated luminosity of 2 ab^{-1} with polarized beams, is comparable to that of 5 ab^{-1} with unpolarized beams, with most of the improvement coming from e^- polarization alone [24]. The main effect of beam polarization is to discriminate the effect of different SMEFT operators that contribute to the Higgs boson coupling. There is a similar gain of a factor of about 2.5 from discrimination of the effects of the operators contributing to the $WW\gamma$ and WWZ couplings, which also enter the SMEFT analysis. The positron polarization becomes more relevant at higher center-of-mass energies. For instance, W-boson fusion reactions, such as $e^+e^- \to \nu\bar{\nu}H$, proceed only from $e^-_L e^+_R$ initial states, providing a cross-section (or, equivalently, effective luminosity) enhancement of approximately 2.5 for typical polarizations foreseen at future linear e^+e^- machines [12]. Here positron polarization makes a significant contribution. This implies that the same number of Higgs bosons can be produced through this process with only approximately 40% of the integrated luminosity, compared with having unpolarized beams.

Direct measurement of CP-odd observables would unambiguously establish CP violation in the top quark–Higgs boson coupling. This is challenging at the Large Hadron Collider (LHC) due to the inability to fully reconstruct the $t\bar{t}H$ system. The use of polarized beams has been shown to boost the sensitivity to the CP structure of the top quark–Higgs boson coupling in combined measurements of the total cross section of $e^+e^- \to t\bar{t}H$ production [25] and related CP-violating observables. These direct probes are complementary to model-dependent constraints on CP-mixed fermion–Higgs boson couplings from measurements of electric dipole moments [26].

Moreover, beam polarization at high energy enables the suppression of relevant backgrounds, such as the dominant $e^+e^- \to W^+W^-$ background for positive (negative) electron (positron) beam polarization, increasing the signal-over-background ratio and allowing the precise measurement of the rate of other backgrounds, as well as the reduction of detector-related systematic uncertainties, with combined measurements of datasets with four distinct initial-state polarization configurations. These effects collectively indicate the increased precision reach that beam polarization provides for linear machines [12].

For these reasons, in this analysis we propose a comparison of the carbon footprint of collider concepts relative to their expected precision in Higgs boson coupling measurements. Table II summarizes the projected relative precision for Higgs boson coupling measurements at each collider combined with projected results from the High-Luminosity Large Hadron Collider (HL-LHC). As can be seen, the overall physics reach of all proposed Higgs factories is similar [1,23] for operation at 240–250 GeV, and additional measurements become accessible for the higher center-of-mass energy runs at linear colliders. We also compare the Higgs factory proposals in terms of total energy consumption and carbon emissions, for both construction activities and operation, which is the most relevant quantity when one is evaluating each project's impact on the global climate.

We then present an estimate of energy consumption and carbon footprint per unit of physics output. This is achieved by our taking the average of the relative precision over all Higgs couplings, weighting them by the relative improvement in their measurement with respect to the HL-LHC:

$$\left\langle \frac{\delta\kappa}{\kappa} \right\rangle = \frac{\sum_i w_i \left(\frac{\delta\kappa}{\kappa}\right)_i}{\sum_i w_i}, \tag{1}$$

TABLE II. Relative precision (%) of Higgs boson coupling and total Higgs boson width measurements at future colliders when combined with the HL-LHC measurements. Results are from Ref. [23]. The FCC-ee numbers assume two interaction points (IPs) and 5 ab^{-1} at 240 GeV and 1.5 ab^{-1} at 365 GeV. The CEPC numbers also assume two IPs, but 20 ab^{-1} at 240 GeV and 1 ab^{-1} at 360 GeV. The top quark Yukawa coupling can be measured with nearly double the precision at C^3 operations at 550 GeV, compared to the ILC operating at 500 GeV, because of the higher center-of-mass energy [27]. Nevertheless, in this study we assume the same precision for C^3 as for the ILC at 500 GeV. Note that since there are no beyond the Standard Model decays allowed in this table, the width is constrained by the sum of the Standard Model contributions. Entries with three dots correspond to couplings that are out of reach ($hc\bar{c}$ at the HL-LHC) or for which estimates were not available at the time of writing (hhh for the CEPC). The weighted average shown in the last row was calculated as explained in the main text.

		HL-LHC +				
Relative precision (%)	HL-LHC	CLIC at 380 GeV	ILC at 250 GeV/C^3 at 250 GeV	ILC at 500 GeV/C^3 at 550 GeV	FCC at 240 GeV/360 GeV	CEPC at 240 GeV/360 GeV
hZZ	1.5	0.34	0.22	0.17	0.17	0.072
hWW	1.7	0.62	0.98	0.20	0.41	0.41
$hb\bar{b}$	3.7	0.98	1.06	0.50	0.64	0.44
$h\tau^+\tau^-$	3.4	1.26	1.03	0.58	0.66	0.49
hgg	2.5	1.36	1.32	0.82	0.89	0.61
$hc\bar{c}$	...	3.95	1.95	1.22	1.3	1.1
$h\gamma\gamma$	1.8	1.37	1.36	1.22	1.3	1.5
$h\gamma Z$	9.8	10.26	10.2	10.2	10	4.17
$h\mu^+\mu^-$	4.3	4.36	4.14	3.9	3.9	3.2
$ht\bar{t}$	3.4	3.14	3.12	2.82/1.41	3.1	3.1
hhh	50	50	49	20	33	...
Γ_{tot}	5.3	1.44	1.8	0.63	1.1	1.1
Weighted average	...	0.94	0.86	0.45	0.59	0.49

where the sum runs over the entries in each column of Table II and the weight is defined as

$$w = \frac{\left(\frac{\delta\kappa}{\kappa}\right)_{\text{HL-LHC}} - \left(\frac{\delta\kappa}{\kappa}\right)_{\text{HL-LHC+HF}}}{\left(\frac{\delta\kappa}{\kappa}\right)_{\text{HL-LHC+HF}}}. \quad (2)$$

This definition weights measurements by their relative improvement over the HL-LHC measurements when the HL-LHC and future HF results are combined. Qualitatively, measurements that minimally improve those of the HL-LHC are assigned weights near zero, while HF measurements with high precision or large improvement over the HL-LHC measurements are assigned larger weights. While other weighting schemes could be used, we argue that Eq. (2) is unbiased towards the type of physics measurement (e.g., Yukawa coupling, self-coupling, or vector coupling) and it emphasizes the individual strengths of each collider facility.

For the estimation of the weighted average precision, the $hc\bar{c}$ coupling was excluded, since there is no estimate for the HL-LHC, whereas we assume that the hhh coupling for the CEPC can be measured with the same precision as for the FCC. The weighted average precision for each collider is given in the last row of Table II.

IV. POWER CONSUMPTION AND OPTIMIZATION

The most obvious way to reduce the carbon impact of a major facility is to minimize the amount of power that it consumes, thereby minimizing the associated emissions from energy production. This is firmly within the means of the facility designers and crucially does not rely on grid electrification. The nominal operating parameters for C^3 operating at 250 GeV are given in Table III.

Several avenues can be pursued to optimize operational power requirements. Increases in luminosity or reduction in power consumption are possible through the development of ancillary technology by increasing the rf source efficiency, increasing the efficiency of powering the accelerating structures, or modification of beam parameters to increase luminosity. At present, the main linac requires approximately 100 MW of power, with 40 MW for the rf sources and 60 MW for the cryogenic system.

For the rf sources, the C^3 concept uses an overall rf system efficiency of 50%, which is in line with present high-power rf sources that are designed with efficiency in mind. However, significant advances in modern design techniques for klystrons are increasing the klystron amplifier's ultimate efficiency significantly with the inclusion of higher-order-mode cavities, multicell outputs, and advanced multidimensional computational tools.

TABLE III. Estimated electrical power requirements for C^3 operating at 250 GeV at nominal luminosity.

Parameter	Value
Temperature (K)	80
Beam loading (%)	45
Gradient (MeV/m)	70
Flat top pulse length (μs)	0.7
Total beam power (MW)	4
Total rf power (MW)	18
Heat load at cryogenic temperature (MW)	9
Electrical power for rf (MW)	40
Electrical power for cryocooler (MW)	60
Accelerator complex power (MW)	≈50
Site power (MW)	≈150

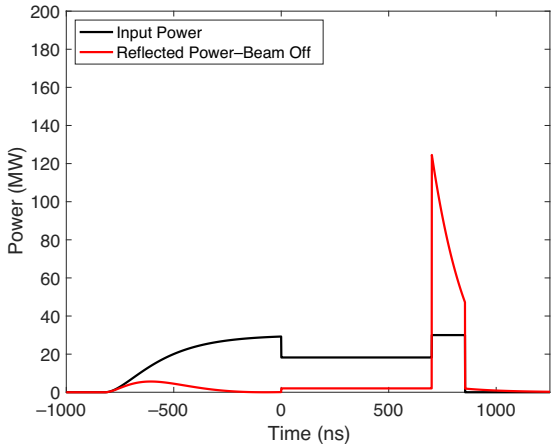

FIG. 1. Forward and reflected power for 1 m of structure for operation at at 70 MeV/m. An rf pulse is shown in the absence of the beam. With the beam the flat top power is constant at 30 MW.

For example, designs now exist for a 50 MW class rf source [28] approaching an amplifier efficiency of 70%. Multibeam rf sources, reducing the beam perveance, have rf source designs exceeding 80% efficiency [29]. These results reinforce modern understanding of the limits of klystron efficiency [30], which indicate a klystron amplifier efficiency of 70–80% is possible, leading to an overall rf source efficiency of 65%.

Radio-frequency pulse compression, presently not in the C^3 baseline, is also a well-known technique for powering high-gradient structures. For C^3, pulse compression is particularly useful due to the impact of power loss at cryogenic temperatures and due to the relatively long fill time for a copper structure operating at cryogenic temperatures. In a previous study [13], it was found that low factors of pulse compression, which preserves rf efficiency in the compressor [31], increase the overall efficiency of the system by 30%. Recently, additional efforts have been made to realize the extremely high Q cavities required for pulse compression with cryogenically cooled rf structures [32,33]; these include concepts operating at room temperature and inside the cryostat at 80 K.

For the baseline C^3 design [9,10] we anticipate operation with 700 and 250 ns flat tops, respectively, for gradients of 70 and 120 MeV/m and a constant power dissipation of 2.5 kW/m at 120 Hz. Figures 1 and 2 show the rf power, dissipated energy, and gradient during the pulse. While these flat top lengths were selected to limit the challenges of breakdown, increasing the flat top length and reducing the repetition rate should be investigated so as to reduce the thermal load on the linac. At present, the thermal balance between the structure fill/dump time and the flat top is approximately 50% (equal thermal load). If we were to extend the flat top lengths by a factor of 2 and reduce the repetition rate by a factor of 2, the thermal dissipation in the main linac would decrease by 25%. This improvement would have little effect on the overall design of the accelerator, and would be acceptable if the breakdown rates remain low enough. Proving that this is possible will require high-gradient testing of structures with 1400 and 500 ns, respectively.

The beam current of C^3 is relatively low because of the large bunch spacing and efficient accelerating structures. One could pursue the possibility of reducing the bunch spacing to increase the current. However, this will require compatibility studies with the detector design. Here we consider the scenario where the bunch spacing is reduced by a factor of 2. This would keep a bunch spacing of more than 1 ns for C^3 operating at both 250 and 550 GeV, resulting in a decrease of 25% for the cryogenic power. The rf power required would decrease by only 20% because the peak rf power required would be slightly higher during the rf pulse flat top to compensate for the additional current.

We note that these approaches can all be combined for mutual benefit as shown in the last row of Table IV. The demonstration research and development plan [11] will be able to investigate these approaches and will lead to potential power savings.

The research and development needed to increase the operational efficiency of C^3 is recognized in the rf technology and beam physics community road maps for the U.S. Department of Energy [15,34,35].

V. CARBON IMPACT OF CONSTRUCTION

Under the assumption that the electric grid will be successfully decarbonized by 2040, as is the goal of many international climate plans, construction, rather than operation, may well dominate the climate impact of a new particle physics facility [5]. For the FCC it is projected that the whole accelerator complex [36] will have a carbon impact similar to that of the redevelopment of a neighborhood of a

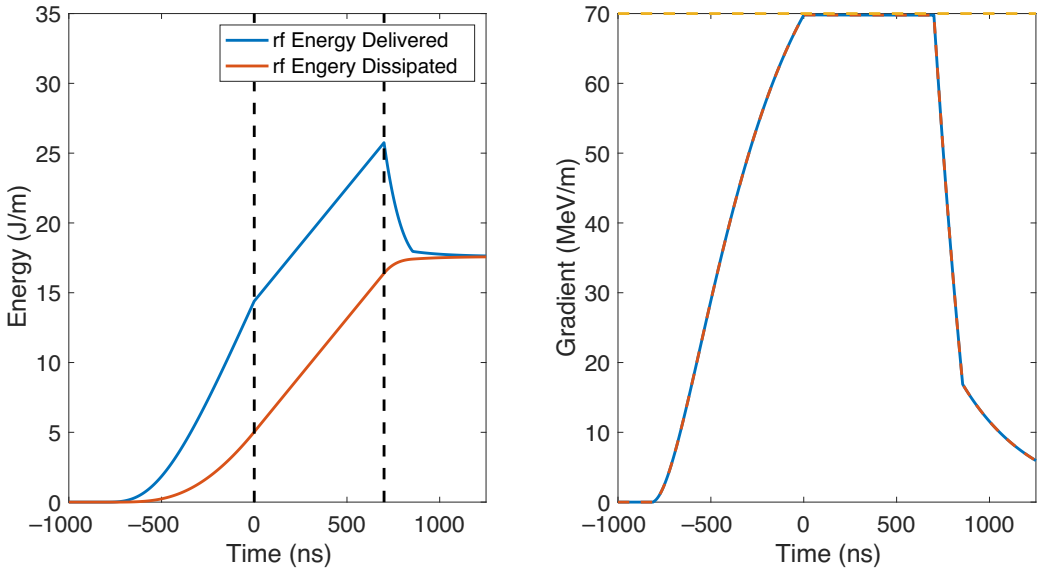

FIG. 2. Dissipated energy per pulse per meter (left) and the time domain gradient (right) in the structure for a 70 MeV/m flat top for 700 ns.

major city [5]. This indicates that the environmental impact of any future collider facility is going to receive the same scrutiny as that of a major urban construction project. The bottom-up analysis in Ref. [5] derives an estimate of global warming potential (GWP) for the manufacture of the main tunnel material (concrete) alone to be equivalent to the release of 237 kton of CO_2 (CO_2e). An alternative top-down analysis is instead dependent on the character of the earth to be excavated, leading to estimates ranging from 5 to 10 kton CO_2e per kilometer of tunnel construction and total emissions of 489–978 kton CO_2e [37].

A life cycle assessment of the ILC and CLIC accelerator facilities is being performed by ARUP [8] to evaluate their holistic GWP, so far providing a detailed environmental impact analysis of construction. The components of construction are divided into classes: raw material supply, material transport, material manufacture, material transport to work site, and construction process. These are labeled A1 through A5, where A1–A3 are grouped as material emissions and A4 and A5 are grouped as transport and construction process emissions. The total GWP for the ILC and CLIC is 266 and 127 kton CO_2e [8], respectively [38]. The approximate construction GWP for the main tunnels is 6.38 kton CO_2e/km for CLIC (5.6 m diameter) and 7.34 kton CO_2e/km for the ILC (9.5 m diameter); the FCC tunnel design is similar to that of CLIC, so 6.38 kton CO_2e/km is used for the calculation of emissions for both the FCC and the CEPC. While a comprehensive civil engineering report is unavailable for the FCC and the CEPC, we estimate the concrete required for the klystron gallery, access shafts, alcoves, and caverns to contribute an additional 30% of emissions, similar to what is anticipated for CLIC. The analysis indicates that the A4 and A5 components constitute 20% for CLIC and 15% for the ILC. In the absence of equivalent life cycle assessment analysis for the FCC and the CEPC, we account for the A4 and A5 contributions as an additional 25%. A summary of these parameters is given in Table V.

The C^3 tunnel will be about 8 km long with a rectangular profile in each of its component systems. Assuming a cut-and-cover approach, all the excavated material will be replaced to yield a small berm. We estimate that for the

TABLE IV. Power savings with adjustment of the main linac design and beam parameters. For 550 GeV, the percentage savings would be unchanged for a combined 79 MW reduction in electrical power from the nominal 125 MW for the main linac.

Scenario	rf system (MW)	Cryogenic system (MW)	Total (MW)	Reduction (MW)
Baseline 250 GeV	40	60	100	...
rf source efficiency increased by 15%	31	60	91	9
rf pulse compression	28	42	70	30
Double flat top	30	45	75	25
Halve bunch spacing	34	45	79	21
All scenarios combined	13	24	37	63

TABLE V. Summary of GWP for different collider proposals separated by origin. Note that FCC and CEPC emissions are estimated on the basis of the comprehensive life cycle assessment of the ILC and CLIC, whereas those of the ILC and CLIC are directly quoted from the ARUP report [8]. The assumptions for the C^3 estimate are discussed in the main text.

		GWP (kton CO_2e)		
Project	Main tunnel length (km)	Main tunnel	Plus other structures	Plus A4 and A5
FCC	90.6	578	751	939
CEPC	100	638	829	1040
ILC	13.3	97.6	227	266
CLIC	11.5	73.4	98	127
C^3	8.0	133	133	146

whole accelerator complex only about 50 000 m^3 of spoil for the experimental hall will have to be relocated. Figure 3 shows a schematic of the C^3 cross section, where the klystron gallery is situated directly above the accelerator hall, with sufficient concrete shielding to allow constant access to the klystron gallery during operation. The application of a top-down estimate of 6–7 kton CO_2e/km obtained from the ARUP report is not appropriate for the C^3 surface site due the differing cross section geometries of the accelerator housing. To allow a fair comparison among facilities, we use the same basic assumptions for construction materials. In particular, that construction uses a mix of CEM1 C40 concrete and 80% recycled steel, the GWP of concrete is taken to be 0.18 kg CO_2e /kg concrete with density 2400 kg/m^3 [39], and 85% of emissions originate from concrete production and 15% of emissions originate from steel production. Taking into account construction of the main linacs, injector linacs, damping rings, beam delivery system, and experimental hall, we estimate the total volume of construction material to be about 260 000 m^3 (consisting mostly of concrete by volume). This leads to a GWP of 133 kton CO_2e for A1–A3 components and GWP per unit length of the main linac of around 17 kton CO_2e/km. Notably, this is roughly a factor of 2 larger than the GWP per kilometer of main tunnel construction of the ILC and CLIC; this suggests further tunnel geometry optimization is achievable with a detailed engineering study. The surface site construction eliminates the need for additional infrastructure (e.g., access tunnels and turnarounds) and greatly reduces the complexity of the construction process, which we estimate to contribute an additional 10% [40] to the GWP. This yields a final estimate of 146 kton CO_2e for civil engineering.

Unlike other Higgs factories under evaluation, the C^3 site has not been decided yet. A C^3 e^+e^- collider could, in principle, be sited anywhere in the world. A community decision will be made regarding the actual site selection, although we note that C^3 offers a unique opportunity to realize an affordable energy frontier facility in the USA in the near term and the entire program could be sited within the existing U.S. National Laboratories. The C^3 tunnel layout would be adapted to its location, and a cut-and-cover site, suitable for a horizontal layout, is extremely attractive also for both cost and schedule reasons. The details of the siting options at Fermi National Accelerator Laboratory are discussed in Ref. [41]. Sites such as the U.S. Department of Energy Hanford site located in the Pacific Northwest have room to accommodate even bigger footprint machines within their site boundary.

VI. MITIGATION STRATEGIES FOR OPERATION

There can be considerable emissions associated with the production of energy required to meet site operation power requirements. This is highly dependent on the region in which the project operates; regions with highly decarbonized electricity grids (via solar, wind, hydroelectric, and nuclear power) offer significantly reduced carbon emissions related to energy production in comparison with those running on nonrenewable energies (gas, oil, and coal). The total emissions of each collider project are then evaluated as the product of the total amount of energy consumed and the local carbon intensity for its production. Increasing the sustainability of the ILC and CLIC has been a significant point of emphasis since the publication of their technical design report [42] and conceptual design report [43], respectively. Here we incorporate the latest published updates for the ILC [12] and CLIC [44] running scenarios that both reduced the operating power requirements significantly.

While total decarbonization of the electric grid by 2040 is a nominal goal, it is not assured. The 2040 projection of carbon intensity based on the stated policies scenario for Japan, China, the European Union, and the USA is roughly 150, 300, 40, and 45 ton CO_2e/GW h, respectively [45]. However, local variations in implementation of renewable energy systems is ignored in these estimates; for example, the CERN-based colliders could take advantage of a 50:50 mix of renewable energy and nuclear energy. Additional mitigation strategies, such as construction of dedicated renewable energy plants, would reduce the carbon impact of operation in other regions. This strategy has been thoroughly investigated by the Green ILC Project [6]. A

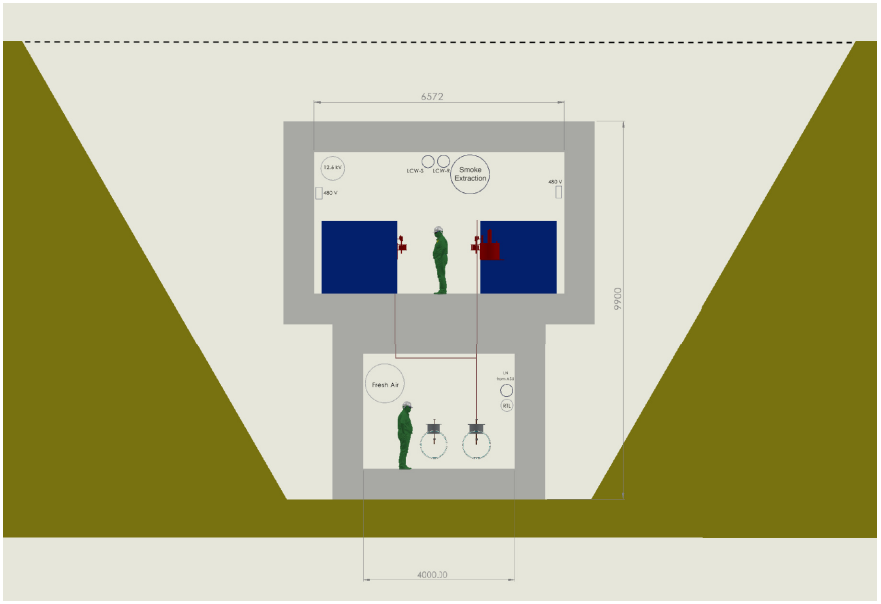

FIG. 3. Layout of the C^3 klystron gallery (upper level) and accelerator hall (lower level) in the cut-and-cover construction approach, which is used for both the main linac and injectors. All dimensions are in mm. Key components of physical infrastructure are shown. The dashed line shows the ground level. All the excavated material will be placed to yield a small berm. Possible locations for Low Conductivity Water Supply (LCW-S), Low Conductivity Water Return (LCW-R), Liquid Nitrogen make up (LN) from the Air Separation Unit (ASU), and the Ring to Linac return line for the damped 10 GeV beam (RTL) are shown.

more moderate strategy can be envisioned for C^3. A 185 MW solar farm could be built with a \$150 million budget [46], double covering the average power requirement of C^3 [47], such that excess power could be stored for later use at night [48], allowing C^3 to achieve green energy independence. The use of multijunction photovoltaic cell fabrication techniques would increase power conversion efficiency well beyond the 30% that is common in today's cells [49], allowing such a solar farm to be situated on about 5 km^2 of land [50].

This estimate relies on energy storage systems supported by regional electricity grids. To better understand the feasibility of scaling all parts of energy production (which may fall under the C^3 project budget) and energy storage infrastructure (which would be funded by the U.S. government, but would nonetheless need investment), we perform a holistic cost estimate. We first note that the energy storage capacity required to supply 150 MW continuously for 12 h is less than 1% of the expected grid energy storage capacity in 2040 [51], indicating that the U.S. grid should be able to reasonably support operation at this scale using renewable energy. We assume lithium ion batteries [52] are the primary energy storage technology with a lifetime of 1000 cycles, experiencing 300 cycles per year, with 10% of battery cost reclaimed through recycling at a base cost of \$125/kWh and \$100/kWh in 2040 and 2050, respectively [53]. We take the cost of solar energy production to be \$0.80/W [50] and take that of onshore, fixed-bottom offshore, and floating offshore wind turbines to be around \$1.3/W, \$3.25/W, and \$5.3/W, respectively [54,55]. An energy production portfolio that provides continuous power for C^3 over a 12 h day and 12 h night period based on these technologies alone would cost approximately \$1 billion. This estimate is primarily driven by requirements of battery energy storage systems and holds for a variety of energy source mixes. This indicates a

TABLE VI. For each of the Higgs factory projects considered in the first row, the center-of-mass energies (second row), ac site power (third row), annual collision time (fourth row), total running time[a] (fifth row), instantaneous luminosity per interaction point (sixth row), and target integrated luminosity (seventh row) at each center-of-mass energy are given. The numerical values were taken from the references mentioned in the table in conjunction with Ref. [19]. For the CEPC the new baseline scenario with 50 MW of synchrotron radiation power per beam is used. We consider both the baseline and the power optimizations from Table IV (in parentheses) for C^3 power requirements.

Higgs factory	CLIC [44]	ILC [12]		C^3 [11]		CEPC [59,60]				FCC [20,61,62]					
$\sqrt{s}$ (GeV)	380	250	500	250	550	91.2	160	240	360	88, 91, 94		157, 163	240	340–350	365
P (MW)	110	111	173	150 (87)	175 (96)	283	300	340	430	222		247	273	357	
$T_{\text{collisions}}$ [10^7 s/year]	1.20	1.60		1.60		1.30						1.08			
T_{run} (years)	8	11	9	10	10	2	1	10	5	2	2	2	3	1	4
$\mathcal{L}_{\text{inst}}$/IP ($\times 10^{34}$ cm^{-2} s^{-1})	2.3	1.35	1.8	1.3	2.4	191.7	26.6	8.3	0.83	115	230	28	8.5	0.95	1.55
$\mathcal{L}_{\text{int}}$ (ab^{-1})	1.5	2	4	2	4	100	6	20	1	50	100	10	5	0.2	1.5

[a]The nominal run schedule reflects nominal data-taking conditions, which ignore other run periods such as luminosity ramp-up.

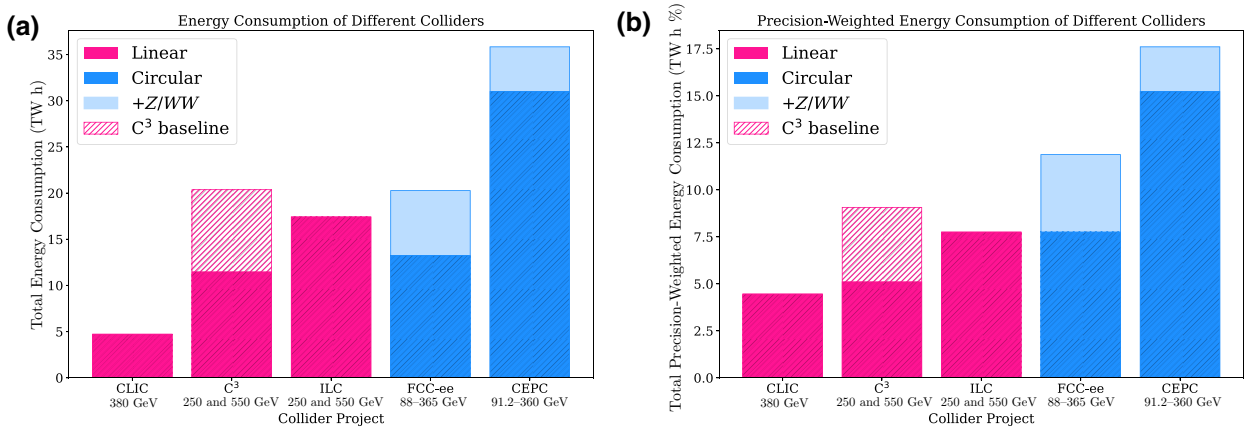

FIG. 4. Total energy consumption for all collider concepts, (a) unweighted and (b) weighted with respect to the average coupling precision for each collider. The hashed pink component represents the additional costs of operating C^3 without power optimization, while light blue regions account for additional run modes targeting Z and WW production.

similar cost would be associated with a site located near the Pacific coast or the Atlantic coast, which could leverage floating and fixed-bottom turbines, respectively, in the southern USA, where solar energy production would be most efficient, or proximate to large wind farms in the Midwest. A more precise cost and feasibility analysis can be performed when a candidate site is defined, as has been done for experiments operating at the South Pole, for example [56]. This cost analysis demonstrates that C^3 operation could be supported sustainably within the USA within the next two decades given conservative projections of technological development.

As a point of comparison, the power requirement of the FCC would be about 30% of the output of a large nuclear plant (generating 1.1 GW on average [57]). At about \$8 billion per facility, the cost of renewable energy infrastructure for the FCC would be about \$2.5 billion. To obtain an estimate of the carbon impact of operation at future collider facilities that takes mitigation strategies into account, we first note that the carbon intensity of solar, wind, hydroelectric, and nuclear energy production is around 30, 15, 25, and 5 ton CO_2e/GW h, respectively [58]. These estimates have some regional variation due to the differences in supply chains and local infrastructure. For instance, given the lifetime of existing nuclear plants of about 30 years, replacement or construction of entirely new facilities will be required and this might effect the overall carbon intensity. While the ultimate energy production portfolio will be different for facilities constructed in different regions, we take a common estimate of 20 ton CO_2e/GW h for all collider facilities in this analysis. We find this to be a reasonable estimate given that any facility can propose mitigation strategies to decouple its carbon impact from the regional average. It also reflects the expectation that clean energy infrastructure supply chains will improve over the next 20 years.

VII. ANALYSIS OF TOTAL CARBON FOOTPRINT

A straightforward calculation of total energy consumption is possible using the information summarized in Table VI, which includes estimates of the site power P during collision mode, the annual collision time $T_{\text{collisions}}$, and the total running time in years T_{run} for each center-of-mass energy $\sqrt{s}$ considered. We take into account the time spent with the beam operating at full rf and cooling power outside data-taking mode, for example, for machine development, as an additional week for every 6 weeks of data-taking (i.e., +17%), represented as $T_{\text{development}}$. We take the site power requirement for the remaining period in a calendar year to be 30% of the site power requirement during data-taking (denoted by κ_{down}). This value is a conservative upper estimate, since without rf power and associated heat load, any accelerator can be kept cold with a small fraction of power to the cryogenic system.

Using these values, we calculate the annual energy consumed as

$$E_{\text{annual}} = P\left[\kappa_{\text{down}} T_{\text{year}} + (1-\kappa_{\text{down}})\right. \\ \left.(T_{\text{collisions}} + T_{\text{development}})\right] \tag{3}$$

and the total energy consumption obtained by summing over all $\sqrt{s}$ run configurations is given by

$$E_{\text{total}} = \sum_{r \in \text{runs}} E(r)_{\text{annual}} T_{\text{run}}(r). \tag{4}$$

For the circular collider projects, the FCC and the CEPC, we consider separately the cumulative energy consumption of the Higgs physics runs (i.e., $\sqrt{s} > 240$ GeV) for a focused comparison on the basis of Higgs physics reach argued in Sec. III, but additionally include the contribution of Z-pole and WW-threshold runs, which impact the climate nevertheless.

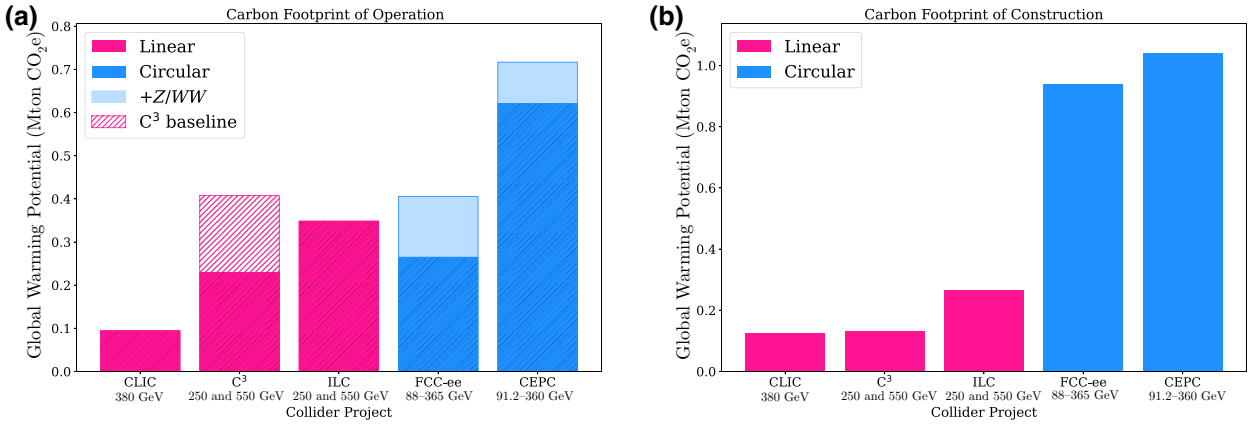

FIG. 5. Global warming potential from (a) operation and (b) construction of all collider concepts. The hashed pink component represents the additional costs of operating C^3 without power optimization, while light blue regions account for additional run modes targeting Z and WW production.

The inclusion of those additional runs enriches the overall physics program of the colliders in a way not reflected in the framework defined in Sec. III. The main purpose of the proposed colliders under consideration here is to serve as Higgs factories, and thus we maintain the importance of assessing their physics reach through the projected precision for Higgs observables. Furthermore, as we demonstrate later, the inclusion of those additional runs does not significantly alter the GWP of the circular machines, which is dominated by construction.

It is worth noting that the FCC-ee tunnel is planned to be reused to host a high-energy hadron collider, while a high-energy machine following C^3 requires additional construction. However, such a hadron collider requires new structures, notably a dedicated superconducting magnet system, along with the disposal of the e^+e^- beamline, which will have been exposed to high levels of radiation. A full life cycle assessment including the carbon impact of the accelerator structures and an end-of-life plan is required to quantify the relative advantage of reusing the tunnel and is beyond the scope of this work.

Figure 4(a) shows the energy consumption for the collider projects considered. The least energy is consumed by CLIC, driven by the lowest planned run time at low energies and its marginally lower power consumption compared with C^3 and the ILC, which have comparable power consumption. The energy consumption of the CEPC is large compared with that of the FCC because it is intended that the CEPC will collect 4 times the integrated luminosity at 240 GeV with an associated tripling of the total run duration.

Figure 4(b) shows the precision-weighted energy consumption for the collider projects considered, estimated by our multiplying the energy consumption from Fig. 4(a) by the average relative precision in the last row of Table II. The shortest run time for CLIC is now compensated by the reduced relative precision, in comparison with C^3 and the ILC, leading to overall closer precision-weighted energy consumption. Similarly, the long proposed run time for the CEPC is now taken into account in conjunction with the improved precision reach, yielding a total weighted energy consumption closer to that of the FCC.

Figure 5(a) shows the associated GWP of the total energy required for operation, obtained by our multiplying the total energy consumption by the respective carbon intensity. The relative performance among the facilities in terms of GWP is identical to their relative performance in total energy consumption, due to the common carbon intensity of 20 ton CO_2e/GWh taken for all facilities.

Figure 5(b) shows the GWP due to construction of accelerator facilities. The carbon footprint is very similar among the linear and circular colliders, which is driven primarily by the total length of the accelerator. Figure 6(a) shows the total GWP from construction and operation. CLIC is the most environmentally friendly option, owing to its lead performance in operation emissions as well as its small footprint. The total GWP of C^3 and the ILC is driven by operation emissions, while that of CLIC, the FCC, and the CEPC is almost entirely driven by construction emissions. Possible reductions in the construction component could be achieved by use of concrete with lower cement content than CEM1 C40 considered in this analysis. Such cases would still leave the FCC GWP dominated by construction processes.

Finally, Fig. 6(b) shows the total precision-weighted GWP from construction and operation, estimated in the same way as the precision-weighted energy consumption in Fig. 4(b). Given the overall similar GWP for CLIC and C^3 and the superior precision reach of C^3 at higher energies, compared with CLIC, C^3 appears to be the most environmentally friendly option when the precision-weighted total carbon footprint is accounted for.

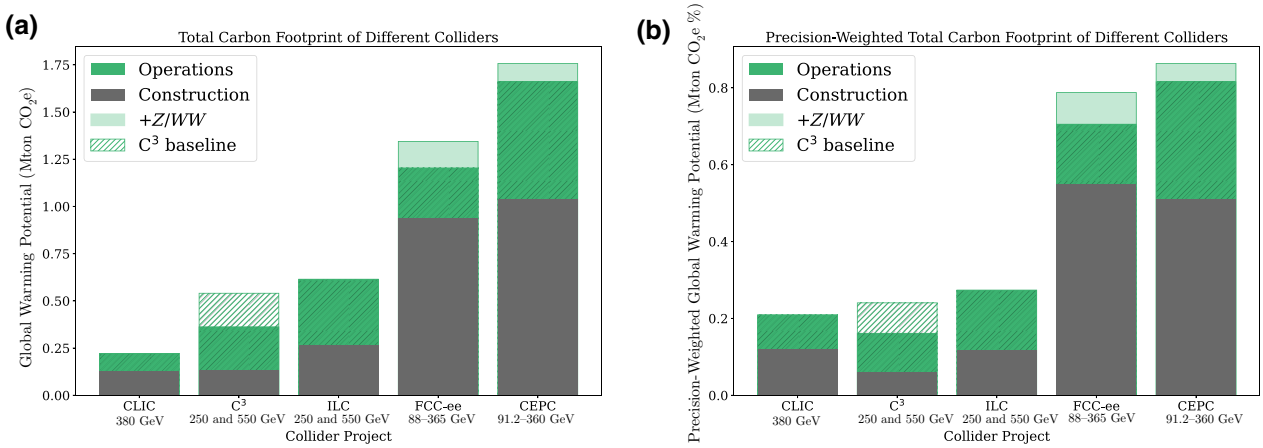

FIG. 6. Total global warming potential from construction and operation for all collider concepts, (a) unweighted and (b) weighted with respect to the average coupling precision for each collider. The hashed pink component represents the additional costs of operating C^3 without power optimization, while light blue regions account for additional run modes targeting Z and WW production.

VIII. CONCLUSIONS

We present the first analysis of the environmental impact of the newly proposed C^3 collider and a comparison with other proposed facilities in terms of physics reach, energy needs, and carbon footprint for both construction and operation.

The physics reach of the proposed linear and circular e^+e^- colliders has been studied extensively in the context of the U.S. Snowmass and European Strategy processes. We focus on the precision of Higgs boson coupling measurements achievable at C^3, CLIC, the ILC, the FCC, and the CEPC. We point out that in terms of physics reach, all the proposed machines are generally similar, although linear colliders can operate at higher collision energies, enabling access to additional measurements of the Higgs boson's properties. Moreover, the use of polarization at linear facilities effectively compensates for the lower luminosity.

On this basis, the global warming potential of these facilities is compared in terms of absolute environmental impact and in terms of environmental impact per unit of physics output obtained by a weighted average of expected precision on Higgs boson coupling measurements. The operation emissions of C^3 could be reduced through beam parameter optimization leading to 63 MW (79 MW) power reduction compared with the nominal 150 MW (175 MW) in the 250 GeV (550 GeV) running mode. Mitigation strategies using dedicated renewable energy facilities can reduce the carbon intensity of energy production to 20 ton CO_2e/GW h. We find that global warming potential is driven by construction rather than by operation beyond 2040. The compact nature of linear collider facilities reduces the total volume of construction materials and opens up the option for a surface site to simplify the construction process. We conclude that linear colliders and C^3 in particular have great potential for an environmentally sustainable path forward for high-energy collider facilities.

ACKNOWLEDGMENTS

The authors express their gratitude to Dan Akerib, Tom Shutt, Sridhara Dasu, Patrick Meade, Nigel Lockyer, Sarah Carson and Jim Brau for their insightful discussions, which have significantly contributed to this work. The authors also extend their appreciation to Michael Peskin and Steinar Stapnes for providing feedback on the manuscript. The work of the authors is supported by the U.S. Department of Energy under Contract No. DE–AC02–76SF00515.

[1] M. Narain, L. Reina, A. Tricoli, M. Begel, A. Belloni, T. Bose, A. Boveia, S. Dawson, C. Doglioni, and A. Freitas *et al.*, *The Future of US Particle Physics – The Snowmass 2021 Energy Frontier Report*, arXiv:2211.11084 [hep-ex].

[2] J. N. Butler *et al.*, Report of the 2021 U.S. Community Study on the Future of Particle Physics (Snowmass 2021) summary chapter, in *Snowmass 2021*. 1, 2023. arXiv:2301.06581 [hep-ex].

[3] CFA Panel for Sustainable Accelerators and Colliders Collaboration, T. Roser, Sustainability considerations for accelerator and collider facilities, in *Snowmass 2021*. 3, 2022. arXiv:2203.07423 [physics.acc-ph].

[4] K. Bloom, V. Boisvert, and M. Headley, Report of the Topical Group on Environmental and Societal Impacts of Particle Physics for Snowmass 2021, arXiv:2209.07684 [physics.soc-ph].

[5] K. Bloom, V. Boisvert, D. Britzger, M. Buuck, A. Eichhorn, M. Headley, K. Lohwasser, and P. Merkel, Climate impacts of particle physics, in *Snowmass 2021*. 3, 2022. arXiv:2203.12389 [physics.soc-ph].

[6] *The Green ILC Project*, https://green-ilc.in2p3.fr/home/. Accessed: 2023-06-23.

[7] P. Janot and A. Blondel, The carbon footprint of proposed e^+e^- Higgs factories, Eur. Phys. J. Plus 137, 1122 (2022), arXiv:2208.10466 [hep-ph].

[8] S. Evans and B. Castle, *CLIC and ILC Life Cycle Assessment Final Report*, ARUP Group, 2023. https://edms.cern.ch/document/2917948/1.

[9] M. Bai *et al.*, C^3: A "cool" route to the Higgs boson and beyond, 2021. arXiv:2110.15800 [hep-ex].

[10] S. Dasu, E. A. Nanni, M. E. Peskin, and C. Vernieri *et al.*, Strategy for understanding the Higgs physics: The Cool Copper Collider, in *Snowmass 2021*. 3, 2022. arXiv:2203.07646 [hep-ex].

[11] E. A. Nanni, M. Breidenbach, and C. Vernieri *et al.*, C^3 demonstration research and development plan, arXiv:2203.09076 [physics.acc-ph].

[12] ILC International Development Team Collaboration, The International Linear Collider: Report to Snowmass 2021, arXiv:2203.07622 [physics.acc-ph].

[13] K. L. Bane, T. L. Barklow, M. Breidenbach, C. P. Burkhart, E. A. Fauve, A. R. Gold, V. Heloin, Z. Li, E. A. Nanni, and M. Nasr *et al.*, An advanced NCRF linac concept for a high energy e^+e^- linear collider, arXiv preprint arXiv:1807.10195 (2018).

[14] M. Nasr, E. Nanni, M. Breidenbach, S. Weathersby, M. Oriunno, S. Belomestnykh, E. A. Nanni, H. Weise *et al.*, Experimental demonstration of particle acceleration with normal conducting accelerating structure at cryogenic temperature, Phys. Rev. Accel. Beams **24**, 093201 (2021).

[15] S. Belomestnykh *et al.*, Accelerator technology R&D: Report of AF7-rf Topical Group to Snowmass 2021, arXiv:2208.12368 [physics.acc-ph].

[16] M. Schneider, V. Dolgashev, J. W. Lewellen, S. G. Tantawi, E. A. Nanni, M. Zuboraj, R. Fleming, D. Gorelov, M. Middendorf, and E. I. Simakov, High gradient off-axis coupled C-band Cu and CuAg accelerating structures, Appl. Phys. Lett. **121**, 254101 (2022).

[17] A. M. Robert Barry, *Radiabeam Ongoing Activities and Future Test Capabilities*, https://indico.slac.stanford.edu/event/7315/contributions/4767/.

[18] P. Bambade *et al.*, The International Linear Collider: A global project, arXiv:1903.01629 [hep-ex].

[19] T. Roser, R. Brinkmann, S. Cousineau, D. Denisov, S. Gessner, S. Gourlay, P. Lebrun, M. Narain, K. Oide, T. Raubenheimer *et al.*, On the feasibility of future colliders: report of the Snowmass'21 Implementation Task Force, JINST **18**, P05018 (2023).

[20] G. Bernardi *et al.*, The Future Circular Collider: A summary for the US 2021 Snowmass Process, arXiv:2203.06520 [hep-ex] (2022).

[21] CEPC Accelerator Study Group Collaboration, Snowmass2021 white paper AF3-CEPC, arXiv:2203.09451 [physics.acc-ph].

[22] CLIC accelerator Collaboration, The Compact Linear Collider (CLIC) - project implementation plan, arXiv:1903.08655 [physics.acc-ph].

[23] S. Dawson, P. Meade, I. Ojalvo, and C. Vernieri *et al.*, Report of the Topical Group on Higgs Physics for Snowmass 2021: The case for precision Higgs physics, arXiv:2209.07510 [hep-ph] (2022).

[24] T. Barklow, K. Fujii, S. Jung, R. Karl, J. List, T. Ogawa, M. E. Peskin, and J. Tian, Improved formalism for precision Higgs coupling fits, Phys. Rev. D 97, 053003 (2018), arXiv:1708.08912 [hep-ph].

[25] R. M. Godbole, C. Hangst, M. Mühlleitner, S. D. Rindani, and P. Sharma, Model-independent analysis of Higgs spin and CP properties in the process $e^+e^- \to t\bar{t}\Phi$, The European Physical Journal C **71**, 1681 (2011).

[26] H. Bahl, E. Fuchs, S. Heinemeyer, J. Katzy, M. Menen, K. Peters, M. Saimpert, and G. Weiglein, Constraining the $\mathcal{CP}$ structure of Higgs-fermion couplings with a global LHC fit, the electron EDM and baryogenesis, The European Physical Journal C **82**, 604 (2022).

[27] T. Barklow, J. Brau, K. Fujii, J. Gao, J. List, N. Walker, and K. Yokoya, ILC operating scenarios, arXiv:1506.07830 [hep-ex].

[28] J. Cai, I. Syratchev, and G. Burt, Design study of a high-power Ka-band high-order-mode multibeam klystron, IEEE Trans. Electron Devices **67**, 5736 (2020).

[29] Q. Chao, R. Zhang, Y. Wang, and X. Zhang, Modeling and design of a high-efficiency multibeam klystron, IEEE Trans. Electron Devices **69**, 2625 (2022).

[30] J. Cai, I. Syratchev, and G. Burt, Development of X-band high power high efficiency klystron, in *High Gradient Workshop, Virtual*. (2021).

[31] P. Wang, H. Zha, I. Syratchev, J. Shi, and H. Chen, Rf design of a pulse compressor with correction cavity chain for klystron-based compact linear collider, Phys. Rev. Accel. Beams **20**, 112001 (2017).

[32] E. Snively, V. Borzenets, G. Bowden, A. Krasnykh, Z. Li, B. Loo, C. Nantista, M. Oriunno, S. M. Shumail, and S. Tantawi, Cryogenic accelerator design for compact very high energy electron therapy, in *Proc. LINAC* (2022), p. 62.

[33] M. Schneider, REBCO sample testing for a HTS high Q cavity, in *Proc. IPAC'23*, no. 14 in IPAC'23 - 14th International Particle Accelerator Conference, (JACoW Publishing, Geneva, Switzerland, 05, 2023), p. 2993.

[34] M. Bai, Z. Huang, and S. M. Lund, Summary report of AF1 to Snowmass 2021: Beam physics and accelerator education within the accelerator frontier, arXiv:2209.07668 [physics.acc-ph].

[35] S. Nagaitsev, Z. Huang, J. Power, J.-L. Vay, P. Piot, L. Spentzouris, J. Rosenzweig, Y. Cai, S. Cousineau, M. Conde *et al.*, Accelerator and beam physics research goals and opportunities, arXiv:2101.04107 [physics.acc-ph].

[36] The main tunnel plus the additional buildings on the site and the materials for the accelerator and detectors, assuming a main tunnel length of 97.7 km (the updated FCC design anticipates 91 km).

[37] Contributions from many bypass tunnels, access shafts, large experimental caverns, and new surface sites are excluded.

[38] We use the emission figures associated with the CLIC drive-beam design, which is more efficient than the alternative design using only klystrons for rf power.

[39] BCSA, steel for life, SCI, lightweight C40 CEM 1 data sheet, PE International, 2012. https://steelconstruction.info/The_Steel_Construction_Information_System.

[40] Nearly all spoil from the surface site excavation in the cut-and-cover approach is replaced onto the accelerator housing yielding a small berm. This removes the need to truck large volumes of spoil off-site, which would be done for the tunneled facilities ILC and CLIC. A surface site also eliminates the need to operate a boring machine. We therefore estimate the relative contribution of the A4-A5 component to C^3 construction emissions to be half that of the tunneled facilities.

[41] P. C. Bhat *et al.*, Future collider options for the US, in *Snowmass 2021*. 3, 2022. arXiv:2203.08088 [hep-ex].

[42] C. Adolphsen *et al.*, *The International Linear Collider Technical Design Report - Volume 3.II: Accelerator Baseline Design*, arXiv:1306.6328 [physics.acc-ph] (2013).

[43] M. Aicheler, P. Burrows, M. Draper, T. Garvey, P. Lebrun, K. Peach, N. Phinney, H. Schmickler, D. Schulte, and N. Toge, *A Multi-TeV Linear Collider Based on CLIC Technology: CLIC Conceptual Design Report*. CERN Yellow Reports: Monographs. CERN, Geneva, 2012. https://cds.cern.ch/record/1500095.

[44] O. Brunner *et al.*, The CLIC project, arXiv:2203.09186 [physics.acc-ph] (2022).

[45] International Energy Agency (IEA), *World Energy Outlook 2022*, Licence: Creative Commons Attribution CC BY-NC-SA 4.0, 2022. https://www.iea.org/reports/world-energy-outlook-2022.

[46] SEIA, *Solar Market Insight Report 2021 Q4*, 2021. https://www.seia.org/research-resources/solar-market-insight-report-2021-q4.

[47] This estimate considers the power optimizations in Table IV.

[48] The additional cost of selling and purchasing energy through utility companies can be reduced through special contracts and is ignored here.

[49] T. Hunt, *How to Make Money from Land as a Solar Developer*, 2013. https://www.greentechmedia.com/articles/read/how-to-make-money-from-your-land-as-a-solar-developer#gs.66msmc.

[50] P. R. Brown, P. J. Gagnon, J. S. Corcoran, and W. J. Cole, *Retail Rate Projections for Long-Term Electricity System Models*, Technical Report NREL/TP-6A20-78224, National Renewable Energy Laboratory, Golden, CO, 2022. https://www.nrel.gov/docs/fy22osti/78224.pdf.

[51] P. Denholm and W. Frazier, *Storage Futures Study: Economic Potential of Diurnal Storage in the U.S. Power Sector*, National Renewable Energy Laboratory, 2021. https://www.nrel.gov/docs/fy21osti/77449.pdf.

[52] Lithium ion batteries are not considered to be viable long-term energy storage solutions; instead, technologies such as flow batteries and systems based on mechanical potential energy are favored.

[53] National Renewable Energy Laboratory, *Utility-Scale Battery Storage*, (2022). https://atb.nrel.gov/electricity/2022/utility-scale_battery_storage.

[54] D. Blewett, *Wind Turbine Cost: Worth The Million-Dollar Price in 2022?*, 2021. https://weatherguardwind.com/how-much-does-wind-turbine-cost-worth-it/.

[55] U.S. Department of Energy, *Land-Based Wind Market Report: 2022 Edition*, 2022. https://www.energy.gov/sites/default/files/2022-08/land_based_wind_market_report_2022_ppt.pdf.

[56] S. Babinec, I. Baring-Gould, A. N. Bender, N. Blair, X. Li, R. T. Muehleisen, D. Olis, and S. Ovaitt, Feasibility of renewable energy for power generation at the South Pole, arXiv:2306.13552 [physics.soc-ph] (2023).

[57] Reuters, *France's EDF expects six new nuclear reactors to cost 46 billion euros: Le Monde*, Reuters (11, 2019). https://www.reuters.com/article/us-edf-nuclear-epr/frances-edf-expects-six-new-nuclear-reactors-to-cost-46-billion-euros-le-monde-idUSKBN1XJ074.

[58] *Electricity Maps*, https://www.electricitymaps.com.

[59] H. Cheng *et al.*, The physics potential of the CEPC. Prepared for the US Snowmass Community Planning Exercise (Snowmass 2021), arXiv:2205.08553 [hep-ph] (2022).

[60] C. A. S. Group, Snowmass2021 white paper AF3-CEPC, arXiv:2203.09451 [physics.acc-ph] (2022).

[61] M. Benedikt, A. Blondel, O. Brunner, M. Capeans Garrido, F. Cerutti, J. Gutleber, P. Janot, J. M. Jimenez, V. Mertens, A. Milanese *et al.*, *FCC-ee: The Lepton Collider: Future Circular Collider Conceptual Design Report Volume 2*, CERN, Geneva, 2019. https://cds.cern.ch/record/2651299.

[62] J.-P. Burnet, *Energy and Sustainability for Future Circular Collider*, https://indico.cern.ch/event/1202105/contributions/5434701/.